Development and Testing of a Prototype LOX/propylene Upper Stage Engine

Kay L. Gemba*, Deepak Verma*
and Eric Besnard†

California State University, Long Beach, CA, 90840, USA

The paper discusses the development of a 2000 N thrust liquid oxygen/propylene rocket engine designed to power the upper stage of a Nanosat Launch Vehicle (NLV). The preliminary design is intended for space operations with an expansion ratio of 70. The targeted combustion efficiency is 95% and nozzle efficiency is 98%, corresponding to a specific impulse of 347 s. Consistent with the employed incremental approach, these requirements are relaxed for the first prototype version of the engine in order to conduct a static fire test (SFT) demonstration at sea-level conditions: the expansion ratio of the nozzle is reduced to 4 by truncating the nozzle, the targeted combustion efficiency is 90% and nozzle efficiency is 95%.

Propellants are introduced and mixed in the combustion chamber utilizing an unlike doublet injector element. In addition, film cooling is provided in order to extend the life of the ablative chamber. Ignition is accomplished with a single igniter mounted on the center face of the injector.

CFD analysis has been performed to validate the design and to characterize the engine's performance. Results show that the upper stage engine produces a thrust of 1979 N with an exit Mach number of 4.3, compared to a one-dimensional calculated Mach number of 4.12. Analysis for the truncated prototype indicate a thrust of 1467 N when the predicted value in those conditions is 1270 N. The exit Mach number is determined to be 2.7.

Nomenclature

η_{c^*}	Combustion Efficiency
γ	Ratio of Specific Heats
λ	Nozzle Efficiency
ε	Nozzle Expansion Ratio
c^*	Effective Characteristic Exhaust Velocity
L^*	Characteristic Length
LOX	Liquid Oxygen
M_c	Combustion Chamber Mach Number
O/F	Oxidizer to Fuel Ratio
P_a	Ambient Pressure
P_c	Combustion Chamber Pressure
P_e	Nozzle Exit Presure
P_{sep}	Flow Separation Pressure
T_c	Chamber Temperature
T/W	Thrust to Weight Ratio

*Student, AIAA Student Member.
†Professor, AIAA Senior Member.

I. Introduction

The initial Nanosat Launch Vehicle (NLV) concept was first proposed by Garvey Spacecraft Corporation (GSC) and California State University, Long Beach (CSULB) in 2003 using LOX/ethanol as propellants[1].

The configuration underwent a series of trade studies resulting in a 2-stage pressure-fed LOX densified propylene vehicle, shown in figure 1[2,3,4], capable of placing a 10 kg (22 lbm) payload into a nominal 250-km altitude polar orbit. The chamber pressure is nominally 2 MPa (300 psi) for the first stage and 1 MPa (150 psi) for the upper stage. Other vehicle characteristics are listed in table 1. A schematic of the vehicle is presented in figure 1.

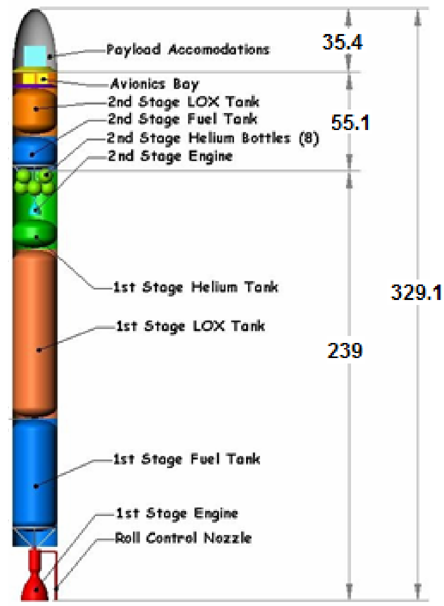

Figure 1: NLV Baseline. Dimensions in cm

Some of the technological characteristics of the NLV are: composite propellant tanks, densified propylene as fuel[5], hot gaseous helium as pressurant, as well as the potential use of carbon/silicon carbide (C/SiC)[6]. A series of developmental static fire tests and flight tests have been conducted, ranging from a low fidelity but full scale first stage to a full scale NLV flight[7,8,9,10]. An evolutionary succession is the Prospector-9 which features a pair of large integral composite tanks instead of the cluster of small 2.85 US Gal tanks used in all earlier vehicles and a 4500 lbf engine that is representative of the NLV first stage engine[17].

Development efforts to date have focused primarily on the first stage and its 20,000 N (4,500 lbf) thrust engine. Some initial static fire tests with room-temperature propylene have been conducted[5]. A concept for the upper stage engine development is presented in this paper at preliminary design stage. The next section describes the development of the engine meeting NLV requirements.

Table 1: NLV Characteristics

	First Stage	Second Stage
Dry mass	171 kg	30 kg
Stage inert mass fraction	0.131	0.137
Chamber Pressure	2 MPa	1 MPa
Sea-Level Thrust	20000 N	N/A
Sea-Level ISP	212 s	N/A
Vacuum Thrust	29600 N	2000 N
Vacuum ISP	314 s	347 s
Seperation/burnout altitude	54 km	250 km

II. Upper stage engine development

A. Engine overview

The engine is compromised of three major subassemblies; the injector, igniter and the combustion chamber assembly. The engine uses LOX/propylene, is pressure fed, operates at a chamber pressure of 1 MPa (approx. 150 psi) and provides a vacuum thrust of 2000 N (approx. 450 lbf). Propylene is chosen as the propellant because it provides a higher specific impulse than RP-1 with comparable density at cryogenic temperatures[15].

A direct spark or a spark torch are likely candidates for the ignition system along with pyrophoric using TEA/TEB. The combustion chamber assembly is built using an ablative liner and a carbon fiber overwrap, while a flat head injector provides additional film cooling to minimize ablation rates. Although the engine is initially designed to use an ablative engine, the configuration can be modified such that the ablative combustion chamber assembly can be replaced with a ceramic matrix composite.

Figure 2 shows the engine with an ablative chamber. The thrust to weight ratio of the engine is required to be above 50. This value is on the lower end and can be significantly increased. The injector weight of the current design can be significantly reduced, however ease of manufacturing is determined to be the primary focus for the prototype. Also, excessive ablative thickness in the nozzle can be removed. Characteristics are summarized in table 2 along with design variables.

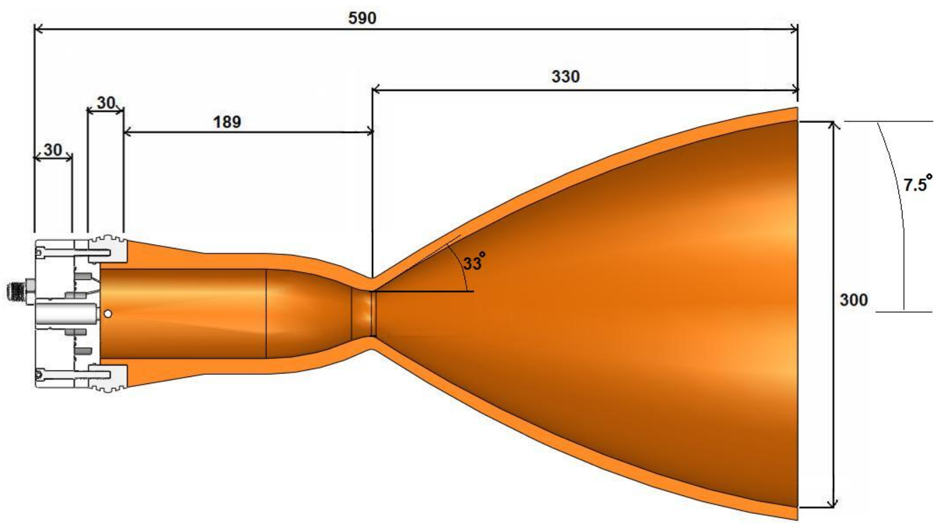

Figure 2: LOX/Propylene Ablative Engine Concepts. Dimensions in mm

Table 2: Upper Stage Engine Characteristics

	Space Engine
minimum T/W requirement	50
ε	70
O/F	2.6
L*	0.8
M_c	0.16

B. Preliminary Performance Estimates

1. *Approach*

MIME and CFD++ have been used to estimate the nozzle performance of the engine preliminary design. Note that section II presents the upper stage engine preliminary design and section III the prototype (for sea-level SFT). A prism layer is included in the axisymmetric mesh at the wall of the engine to accommodate for the boundary layer with an estimated y^+ value of 0.3. The mesh quality was not allowed to drop below a value of 0.3.

For the CFD++ boundary conditions, stagnation pressure and temperature are defined as the inlet conditions, a back pressure imposition of the respective ambient conditions for the outlet condition. The engine wall itself is modeled with an adiabatic viscous wall function. If the run included a boundary which allowed in- and outflow, the boundary condition selected is inflow/outflow characteristic based with the initial conditions.

2. *Baseline performance*

The engine presented in figure 2 has been analyzed in CFD, the initial conditions being space conditions with an ambient pressure close to zero. Figure 3 shows the Mach number plot and figure 4*b* corresponding residuals of the run.

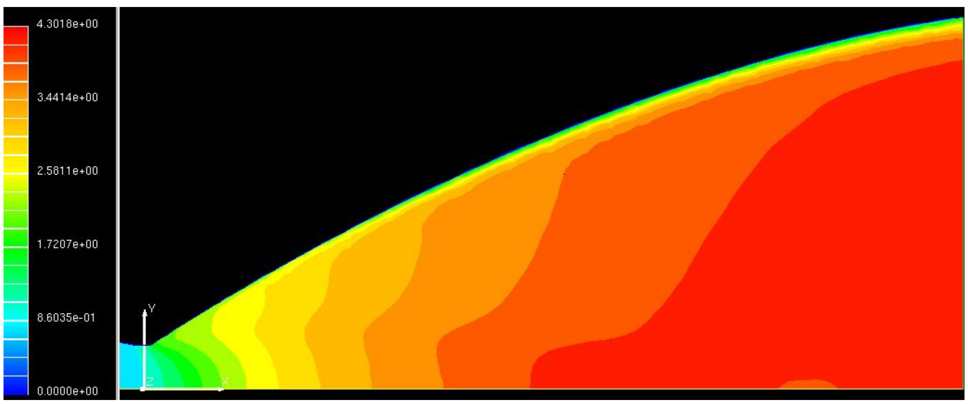

Figure 3: Baseline Mach Number Plot

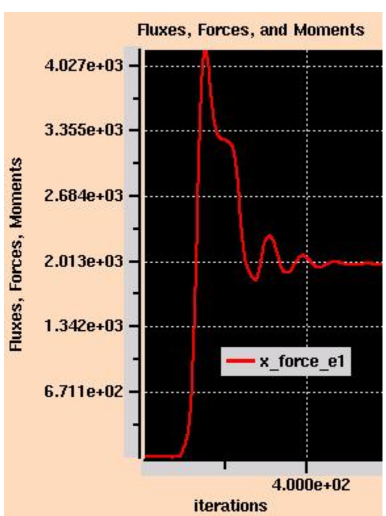

(a) Converging Force Plot in Newton

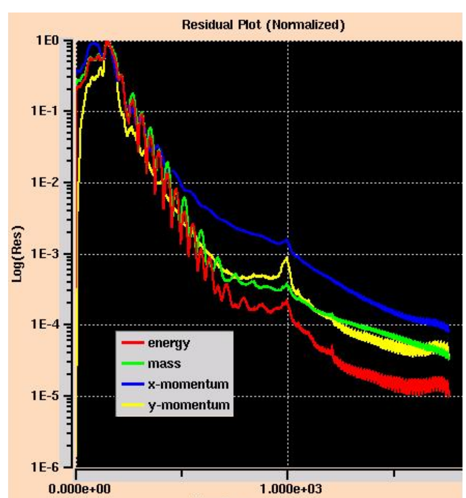

(b) Residuals

Figure 4: Baseline CFD solution convergence

The exit Mach number is determined to be 4.3. As expected, the Mach number is close to the estimate of the one dimensional code, which is computed to be 4.12. The estimated force given by this run is found to be 1979 N, the converging force plot is shown in figure 4*a*. Comparing the CFD force results with the desired thrust of 2000 N and an anticipated nozzle efficiency of .98, the result yields a real nozzle efficiency of 0.7. However, this result neglects wall roughness and divergence loses. Therefore, this estimate needs to be refined after a static fire test is conducted.

3. Next steps

Both the ablative and radiatively cooled chamber designs require the use of some film cooling. This determination will be the subject of future studies. Orifice size and spacing will be analyzed and adjusted if necessary. The impingement on the injector will be slightly adjusted such that all streams converge at the throat of the engine, rather than forming a cylinder as is the case in the current configuration.

To estimate the nozzle performance, frictional losses and divergent losses must be estimated. Roughness estimates will not be modeled in CFD, the actual static fire test will be used to get a better estimate of the prototype engine.

III. Prototype Engine for Sea Level Testing

The development of a prototype version of this engine to be tested at or near sea-level conditions is discussed here. The prototype engine will be truncated for seal level testing, which is very likely to take place at Mojave Desert. Also, due to possible high temperatures at the test site, the engine chamber pressure needs to be adjusted to avoid cavitation in the feedlines and injector. These elements are discussed below.

A. Engine operating conditions

Ambient pressure will be close or higher than 90 kPa. Truncating the engine to an expansion ratio of 4 results to an approximated exit pressure of about 56.5 kPa, which will leave the engine overexpanded. The corresponding exit pressure for an expansion ratio of 3 is determined to be 75kPa, which seems to be the better candidate for this test. Chemical properties of propylene however demand a change in the chamber pressure as discussed below.

The static fire test will be conducted at elevated ambient temperature which can reach 50 degree Celsius. At that temperature, vapor pressure is close to 2.5 MPa[16] which is higher than the nominal upper stage chamber pressure of 1 MPa so that the operating chamber pressure needs to be increased in order to ensure that the fuel stays liquid in the feed system and injector.

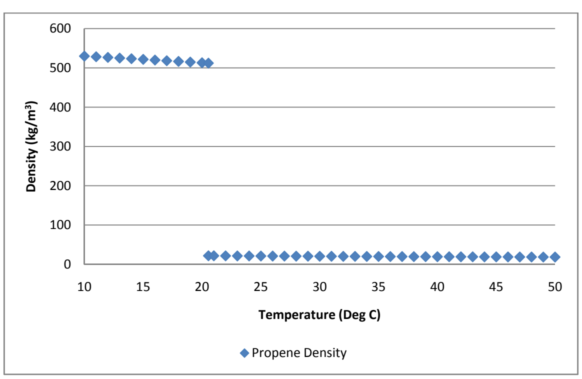

(a) Vaporization Properties of Propene evaluated at 1 MPa

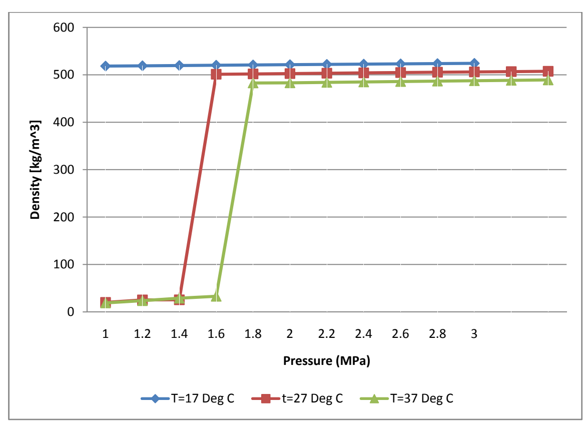

(b) Vaporization Properties of Propene

Figure 5: Propylene physical characteristics

Figure 5*a* shows the behavior of the fuel at chamber pressure conditions, figure 5*b* shows vaporization pressures of propene plotted at three isothermal conditions. The corresponding temperature at which propylene vaporizes at nominal chamber pressure is determined to be close to 21 degree Celsius. Note that for cryogenic temperature, this test problem can be neglected.

Since the test will not be conducted with cryogenic propylene, the chamber pressure will be increased to accommodate for ambient properties, such that the propellant remains in liquid state. Figure 6 displays a likely operation envelope for propylene. Pressure units were converted to psig to accommodate for static fire test stand equipment which is already in place. Statistical data of Mojave suggests that the temperature will be around 43 degree Celsius. Adding a typical delta P of .31 MPa (approx. 45 psi) and another .49 MPa (approx. 72 psi) to account for safety margins and feed losses to the injector results in a minimum tank pressure of 2.35 MPa (approx 340 psi).

In order to cool the propylene down to room temperature, it is possible to place isolation material on the fuel feed system and keep it from warming up. Also, the propylene tanks might be chilled with ice water.

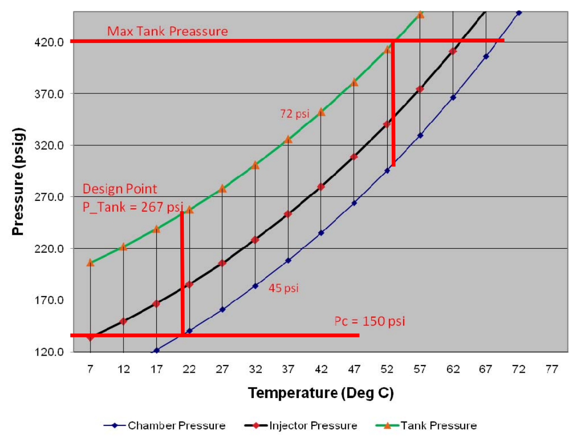

Figure 6: Operation envelope for non cryogenic, liquid Propene and impact on engine operations

B. Prototype Overview

The prototype has a similar configuration to the upper stage engine, however some modifications were necessary. The spark ignition system has been replaced by a pyrotechnic torch which is still center mounted but the electric match used to ignite the pyrotechnic device is fed through the nozzle. Furthermore, the fuel for this test will be at room temperature rather than at cryogenic temperatures. Since the fuel must be liquid when entering the chamber, the chamber pressure will be increased according to ambient conditions. Figure 7 shows a cross section of the prototype engine along with the injector and center mounted igniter.

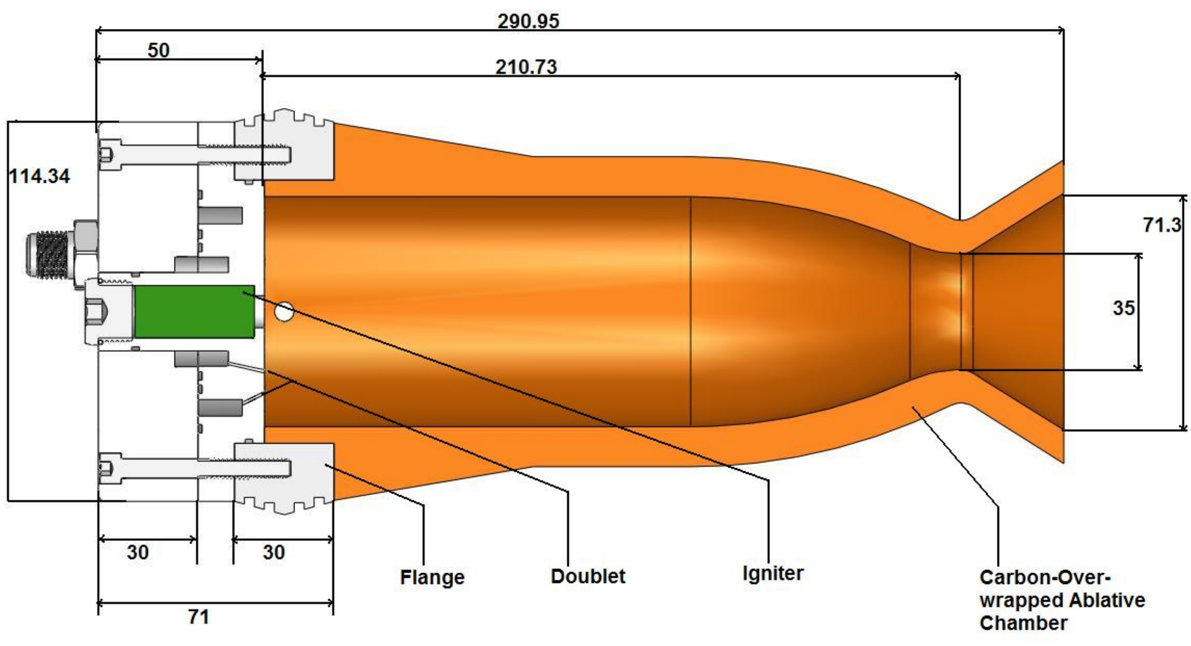

Figure 7: Prototype Cross Section. Dimensions: mm

Table 3 compares characteristics for both the prototype and the upper stage engine.

Table 3: Upper Stage Engine Characteristics

	Prototype (SFT)	Upper Stage Engine
Fuel	room temperature	densified (cryogenic)
Nominal P_c	1.03 MPa	1.03 MPa
Isp	195 s (SFT)	347 s (Vacuum)
P_c range	1.03-2.76 MPa	0.5-1.03 MPa
Thrust	1220-4000 N	1000-2000 N
ε	4	70
λ	0.95	0.98
η_{c^*}	0.90	0.95
c*	1616 m/s	1616 m/s
T_c	3470 K	3470 K
P_e	56,500 Pa	1507 Pa
P_a	90,000 Pa	10 Pa
γ	1.21	1.12

1. Injector

A flat head injector was chosen as the type of injector since it provides good performance than other injectors. It is designed with one set of unlike doublets, 16 % of the fuel is allocated to film cooling. The discharge coefficient is assumed to be 0.8, which will be adjusted after water-flow tests. To reduce pressure coupling between the combustion chamber and the feed system and prevent chugging, the assumed pressure drop between propellant feed system and chamber pressure is assumed to be 30%[11,12] of the chamber pressure. The drop is on the higher end since the upper stage engine will operate in blow down mode (throttled) in its final phase of operation. One of the key design features of the injector is that it can be removed from the chamber without completely disassembling the plates; this greatly reduces engine assembly time and eases integration. The igniter is center mounted. Figure 8 shows the bottom view and figure 9 the side view of the injector. Dimensions for both figures are in mm.

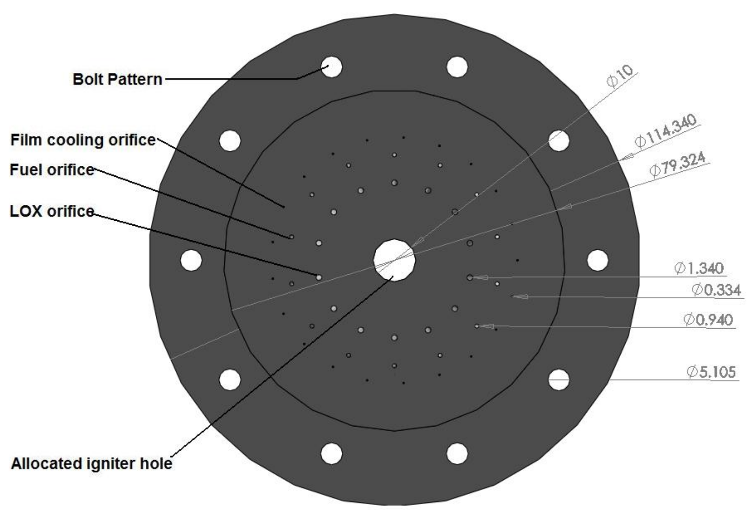

Figure 8: Injector Bottom View

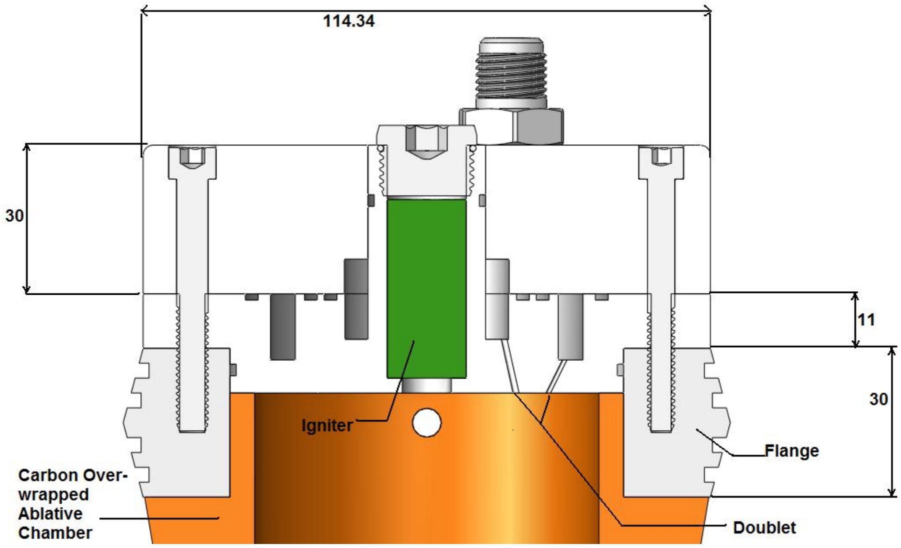

Figure 9: Injector Cross Section View

2. Combustion Chamber Assembly

The combustion chamber and nozzle assembly is an ablative with a silica tape and high temperature epoxy resin. For longer duration burns, silica/phenolic is used. The ablative liner is over-wrapped with carbon fiber epoxy to add extra strength to the chamber and nozzle. The combustion chamber is cylindrical in shape, is 69 mm in diameter and 174 mm long with a 3 degree draft to allow for easy release from the mold used to lay-up the ablative chamber (figure 10). The throat diameter is 35 mm and the exit diameter is 71.3 mm which results in an expansion ratio of 4.

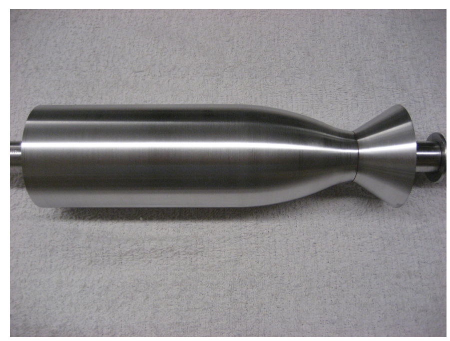

Figure 10: Engine chamber mold

3. Igniter

Ignition for the later NLV first stage engines are accomplished by using several small pyrotechnic lances which were inserted through the nozzle. This represented a scaling up from the ignition configuration employed on smaller engines. Similarly to the larger first stage engine prototype,[17] a pyrotechnic device mounted on the engine is used for ignition. In this case, however, instead of being mounted to the combustion chamber and firing radially inward, the design is such that one igniter is mounted in the center of the injector. The danger of blowing the flame out is relatively low due to a relatively small engine with a mass flow rate of only 0.64 $\frac{kg}{s}$. Figure 9 shows the igniter in green. The port to its right supports a thermocouple probe extending across the injector face to reach the center, right in the exhaust of the igniter. This configuration also facilitates rapid removal and replacement for quick turnaround between tests.

C. Prototype Engine Performance

Performance estimates of the truncated version of the high expansion ratio nozzle are presented within this section. Since the engine is not designed but truncated for an expansion ratio of 4, flow will expand quickly after passing the throat. Exit Mach number is expected to be higher than values given by the ODE code, which should result in an increase of thrust.

1. Injector

Once the injector has been manufactured, impingement is verified with a water-flow test and orifices are adjusted to obtain the desired oxidizer to fuel ratio. Furthermore, the discharge coefficient of the injector will be determined and its pressure drop. Figure 11 shows a previously conducted test.

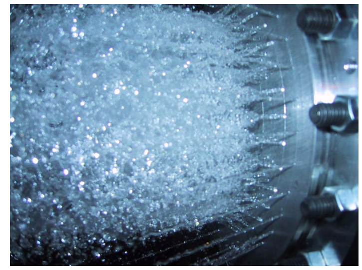

Figure 11: Injector water flow testing

2. CFD

The prototype has been analyzed in a similar way as the upper stage engine with CFD and MIME. Boundary conditions are the same, except for the ambient conditions. The back pressure has been set to 90kPa. First, internal flow solutions are presented in order to be able to investigate the behavior of the flow near the throat. The final envelope of the truncated engine is shown in figure 13*a* along with its Mach number distribution. Note that contour levels have been adjusted for comparison purposes. For reference, converging residuals of this run are show in figure 12*a*. As expected, since the expansion angles are those corresponding to the large expansion ratio engine, the Mach number at the exit is not uniform and reached 2.69, higher than the expected value of 2.5 in a one-dimensional calculation.

The calculated force given by figure 12*b* is determined to be 1467 N, which is higher than the calculated force of 1250 N. As mentioned above, this results can be explained by examining the steep divergent angle behind the throat. Since the engine is initially designed for a bigger expansion, the truncated version expands very quickly. This results in a lower exit pressure as shown in figure 13*b*, being close to 40kPa where separation may occur. Work is now in progress to incorporate the plume in the CFD analysis to investigate this possibility.

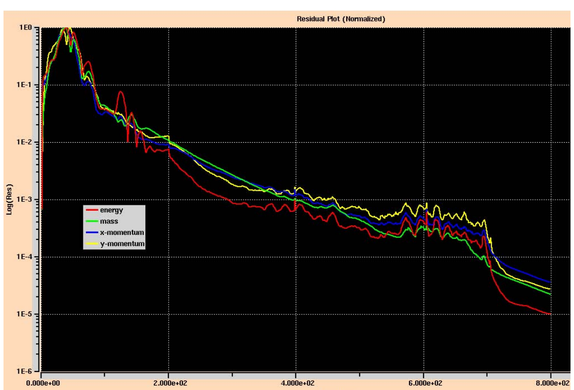

(a) Residuals

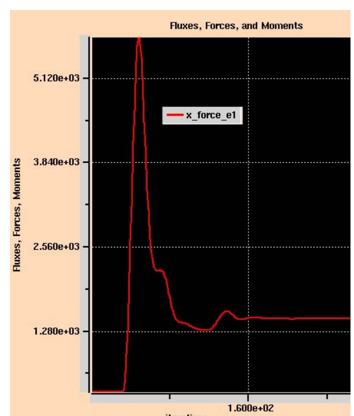

(b) Converging Force Plot in Newton

Figure 12: CFD solution convergence for Sea Level Prototype

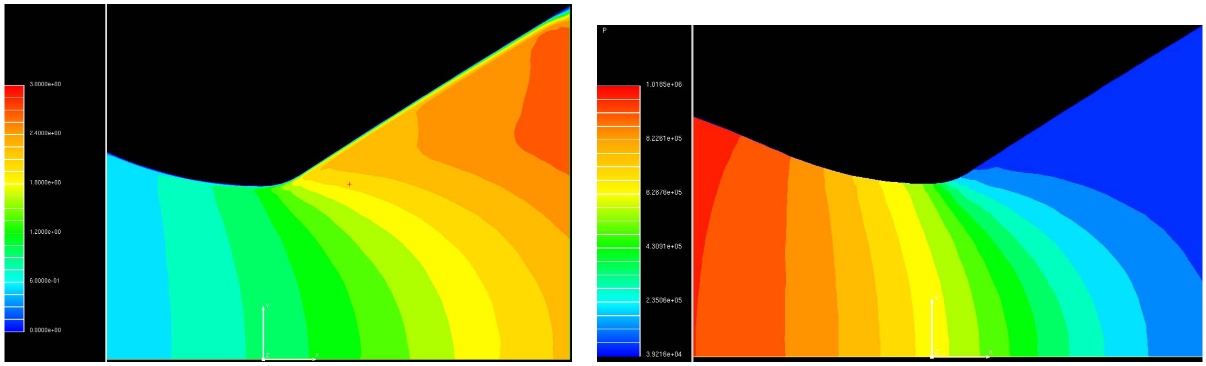

(a) Mach Number Plot (b) Pressure Distribution

Figure 13: CFD solution at $P_c = 1$ MPa

The same CFD analysis has been conducted at an increased chamber pressure of 1.72 MPa (approx. 250 psi) in order to estimate likely test conditions. A summary of the values calculated by the one dimensional code are presented in table 4.

Table 4: Anticipated SFT Engine Conditions

	SFT Engine
ε	4
O/F	2.6
P_c	1.72 MPa
T_c	3547 K
M_e	2.5
γ	1.12

The Mach number distribution is shown in figure 15*a* and converging residuals in figure 14*a*. Contour levels have also been adjusted. The Mach number at the exit is not uniform and reached 2.54, close to 2.50 in the one-dimensional calculation. The calculated force given by figure 14*b* is determined to be 2459 N, which is significantly increased due to the increase in chamber pressure. The exit pressure increased to a value close to 80kPa, shown in figure 15*b*. It seems that the expansion ratio of 4 is the better choice for this test when comparing the exit pressure to the ambient pressure of 90kPa.

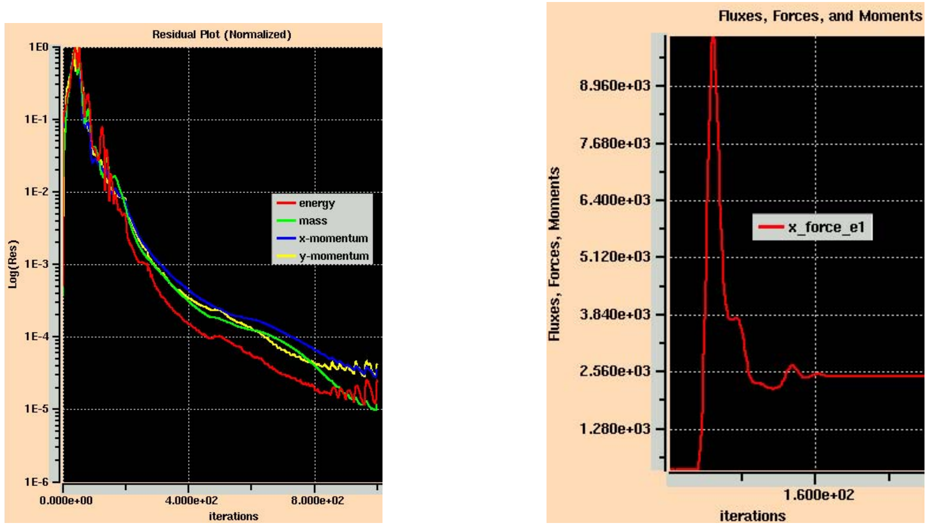

(a) Residuals (b) Converging Force Plot in Newton

Figure 14: CFD solution convergence for Sea Level Prototype

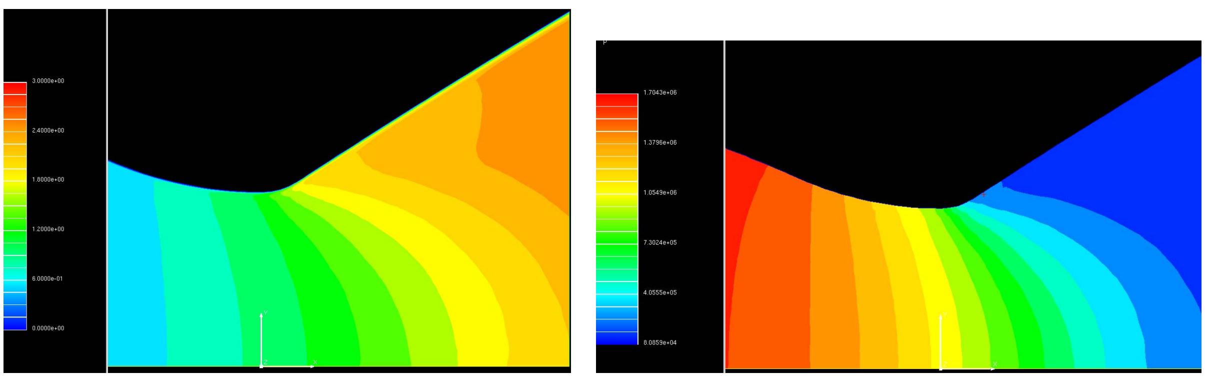

(a) Mach Number Plot (b) Pressure Distribution

Figure 15: CFD solution at $P_c = 1.7$ MPa

D. Next steps

The prototype engine is being manufactured and a static fire test is planned for the summer/early fall 2008. The test data will be used to compare with CFD predictions. Data obtained should be very similar to predictions and the CFD analysis in the previous sections. Further CFD analysis including the plume will be conducted to validate the results and conclusion of this paper. Also, it will be favorable to do some CFD runs with pressure probing files, to plot pressure as a function of location.

IV. Conclusion

The approach presented here follows the incremental development approach employed by the team to leverage existing resources while making progress towards the development of an operational NLV. The paper presents a preliminary design of the NLV upper stage engine and expands on the development of an early prototype to be tested near sea level conditions. Implications on the use of room-temperature propylene and operating at a reduced expansion ratio are discussed, the static fire test will show if the engine design meets nominal performance requirements and is able to successfully power the upper stage of a Nanosat Launch Vehicle.

Next, manufacturing of the prototype will be finalized. The upper stage engine design will be refined to improve performance, such as decreasing the weight of the injector. Ignition for LOX/propylene for in-space condition will then be addressed, which is expected to be similar to that of LOX/methane.

V. Acknowledgments

The team would like to thank the following persons for their help and time: Matt Baker and George Haberstroh. We would also like to thank Associate Student Incorporated (ASI) at CSULB for funding our research with a SURF grant.

References

[1] J. Garvey, E. Besnard, G. Elson and K. Carter, "The Incremental Development of a Cost-Effective Small Launch Vehicle for Nanosat Payloads," AIAA Paper No. 03-6390, presented at Space 2003, Long Beach, CA, Sept. 2003.

[2] J. Garvey and E. Besnard, "A Status Report on the Development of a Nanosat Launch Vehicle and Associated Launch Vehicle Technologies," AIAA Paper No. 04-7003, presented at the 2nd Responsive Space Conference, Los Angeles, CA, April 2004.

[3] J. Garvey and E. Besnard, "Development of a Dedicated Launch System for Nanosat-Class Payloads," Paper No. SSC04-X-3, 18th AIAA/USU Conference on Small Satellites, Logan, UT, Aug. 2004.

[4] J. Garvey and E. Besnard, "Progress Towards the Development of a Dedicated Launch System for Nanosat Payloads," AIAA Paper No. 04-6003, presented at Space 2004, San Diego, CA, Sept. 2004.

[5] J. Garvey and E. Besnard, "LOX-Propylene Propulsion testing for a Nanosat Launch Vehicle," AIAA Paper No. 05-4294, presented at the Joint Propulsion Conference, Tucson, AZ, July 2005

[6] J. Garvey and E. Besnard, "RLV Flight Operations Demonstration with a Prototype Nanosat Launch Vehicle," AIAA Paper 2006-4787, presented at the 42nd Joint Propulsion Conference, Sacramento, CA, July 2006.

[7] J. Garvey and E. Besnard, "Ongoing Nanosat Launch Vehicle Development for Providing Regular and Predictable Access to Space for Small Spacecraft," Paper No. SSC05-X-2, 19th AIAA/USU Conference on Small Satellites, Logan, UT, Aug. 2005.

[8] J. Garvey and E. Besnard, "Initial Results of Nanosat Launch Vehicle Developmental Flight Testing," AIAA Paper 2005-6641, presented at the Space 2005 conference, Long Beach, CA, Aug. 2005.

[9] J. Garvey and E. Besnard, "RLV Flight Operations Demonstration with a Prototype Nanosat Launch Vehicle," AIAA Paper 2006-4787, presented at the 42nd Joint Propulsion Conference, Sacramento, CA, July 2006.

[10] J. Garvey and E. Besnard, "Initial Results from the Demonstration and Analysis of Reusable Nanosat Launch Vehicle Operations," presented at the 54th

[11] Hunzel, Dieter K. (1992). "Modern Engineering for Design of Liquid-Propellant Rocket Engines." Volume 147, Washington DC: AIAA

[12] Humble, Ronald W. (1995) "Space propulsion Analysis and Design" 1th edition, New York: McGraw-Hill Companies, Inc.

[13] Schlichting H. (1979) "Boundary-layer theory." 7th edition, New York: McGraw-Hill Companies, Inc.

[14] "Two Dimensional Kinetic (TDK) Code". 17 May, 2008 `http://www.sierraengineering.com/TDK/tdk.html`

[15] Pioneer Astronautics, "LOX Olefin Rocket Propulsion for Deep Space," proposal abstract, NASA SBIR 02-1 Solicitation, proposal no. 02- S1.02-7918, 05 September 2002

[16] "Chemistry Web Book". 17 May, 2008 `http://webbook.nist.gov`

[17] G. Haberstroh, E. Besnard, M. Baker, and J. Garvey, "Development of a Prototype Rocket Engine for a Nanosat Launch Vehicle First Stage," AIAA Paper No. 2008-4662, July 2008